Cytometry
PART A
Journal of the International Society for Advancement of Cytometry

A Computational Platform for Robotized Fluorescence Microscopy (II): DNA Damage, Replication, Checkpoint Activation, and Cell Cycle Progression by High-Content High-Resolution Multiparameter Image-Cytometry

Laura Furia, Pier Giuseppe Pelicci, Mario Faretta*

Department of Experimental Oncology, European Institute of Oncology, IFOM-IEO Campus for Oncogenomics, Milan 20139, Italy

Received 4 April 2012; Revision Received 9 January 2013; Accepted 22 January 2013

Grant sponsor: Italian Ministry of Health ("Ricerca Corrente"); Grant sponsor: International Association for Cancer Research (AICR); Grant number: 100744; Grant sponsor: Aclon; Grant Sponsor: Fondazione Vollaro

Additional Supporting Information may be found in the online version of this article.

*Correspondence to: Mario Faretta, Department of Experimental Oncology, European Institute of Oncology, IFOM-IEO Campus for Oncogenomics, via Adamello 16, 20139 Milan, Italy.

Email: mario.faretta@ieo.eu

Published online 5 March 2013 in Wiley Online Library (wileyonlinelibrary.com)

DOI: 10.1002/cyto.a.22265

Abstract

Dissection of complex molecular-networks in rare cell populations is limited by current technologies that do not allow simultaneous quantification, high-resolution localization, and statistically robust analysis of multiple parameters. We have developed a novel computational platform (Automated Microscopy for Image CytOmetry, A.M.I.CO) for quantitative image-analysis of data from confocal or widefield robotized microscopes. We have applied this image-cytometry technology to the study of checkpoint activation in response to spontaneous DNA damage in nontransformed mammary cells. Cell-cycle profile and active DNA-replication were correlated to (i) Ki67, to monitor proliferation; (ii) phosphorylated histone H2AX (γH2AX) and 53BP1, as markers of DNA-damage response (DDR); and (iii) p53 and p21, as checkpoint-activation markers. Our data suggest the existence of cell-cycle modulated mechanisms involving different functions of γH2AX and 53BP1 in DDR, and of p53 and p21 in checkpoint activation and quiescence regulation during the cell-cycle. Quantitative analysis, event selection, and physical relocalization have been then employed to correlate protein expression at the population level with interactions between molecules, measured with Proximity Ligation Analysis, with unprecedented statistical relevance. © 2013 International Society for Advancement of Cytometry

Key terms

image-cytometry; cell-cycle; DNA damage response

QUANTIFICATION of cellular DNA damage (DD) is a main target in cancer research (1,2) as genomic instability is a hallmark of most human cancers. Endogenous and exogenous DNA damaging agents continuously threaten the integrity of our genome, but cells have evolved a tightly regulated network of molecular mechanisms to protect it, known as DNA damage response (DDR). Multiple pathways start from the recognition of a single double-strand break (DSB) by the MRN complex (Mre11-Rad50-Nbs1). The activated signaling cascade then leads to differential recruitment of repair effectors according to the type of lesion (3–7).

Localization of damaged sites in the genome is usually based on the detection of the phosphorylation of the histone isoform H2AX (γH2AX) that extends over a broad genomic area around the lesion (8–12). However, accumulating evidence is challenging the notion of a univocal link between serine 139 phosphorylation of H2AX and DNA-breaks (13–17).

Thanks to the increasing availability of antibodies directed towards the DDR molecular machinery, new surrogate markers have been proposed. For example, monitoring of 53BP1 spatial distribution provides a first alternative to γH2AX detection. 53BP1 rapidly relocalizes to DSB sites, activating the ATM-driven signaling cascade (18,19). It plays a fundamental function in nonhomologous end joining

ISAC
International Society for Advancement of Cytometry

(NHEJ) repair, which is mainly active in resting cells and repressed during the S-phase (20). The 53BP1 fundamental role in inducing genomic instability through error-prone repair activation has been recently shown in a mutated BRCA background (21,22). A specific function in the processing of damaged DNA fragile sites has been also attributed to 53BP1 (23,24). Both γH2AX and 53BP1 are essential to activate the cell-cycle checkpoint and to arrest cell cycle progression (25), and their colocalization might be an effective marker of DSBs (26,27). However, due to their participation to multiple DDR and repair pathways, a direct correlation between their expression, localization, and interaction in the different phases of the cell cycle is very much required.

Detection of physiological DD is challenging because of the high sensitivity and spatial resolution required for its quantification. Flow cytometry, laser-scanning cytometry and image-streaming cytometry can all provide statistically significant measurements and have been employed to quantify γH2AX and/or other DDR effectors (8,26,28–34). The recognition and quantification of DD foci by H2AX phosphorylation and/or 53BP1 relocalization demand an image-based approach, but they still represent a challenging task for automatic image processing. In particular, detection and quantification of endogenous DD foci call for the use of high Numerical Aperture (NA) objectives to increase the amount of collected photons and to detect small foci with size close to and below the diffraction limit. Moreover, the molecular crowding typical of the detected signals requires maximal resolution to resolve clusters of foci and to evaluate the colocalization of the involved DDR components. Many efforts have been made to provide efficient computational tools for foci quantification and description (9,27,35–40). However, a high-content image-analysis on a high number of cells is required for results to be statistically significant to: (i) target specific subpopulations, (ii) quantitatively describe phenotypes related not only to DDR but also to checkpoint activation, and (iii) monitor cell-cycle position and progression.

Here, we present a seven-parameter quantitative image-based analysis of the cell cycle with unprecedented spatial resolution and statistical sampling. Combining the flexibility offered by the automation of multiple fluorescence microscopy platforms with our novel analysis software (A.M.I.CO., see the accompanying technical note in this issue), we examined the connections between DDR and cell-cycle checkpoints during exponential cell growth, focusing on the effect of proliferation on genome integrity.

For the first time, we provide a detailed kinetics of both protein content and protein interactions during unperturbed cell-cycle progression. Our results show correlations between DDR and cell proliferation, revealing both accumulation of γH2AX during DNA replication, and colocalization between γH2AX-foci and replication factories. The spatial proximity between γH2AX-foci and the newly replicated DNA, shown by in-situ proximity ligation assay (PLA), indicates the immediate activation of DDR in response to replication errors. We detected distinct expression profiles for γH2AX and 53BP1, together with variable colocalization during the cell-cycle. DDR and checkpoint-activation markers showed either correlated or independent expression profiles. Finally, we show that 53BP1 and γH2AX interact with p53 independently from each other, and that these interactions are quantitatively modulated across the cell cycle.

The data collected contribute to delineate a hierarchy in DDR, providing a most exhaustive view of the complex molecular network regulating tumor-suppressing mechanisms.

Materials and Methods

Cell Culture

MCF10A cells were grown in 50% Dulbecco's Modified Eagle Medium +50% Ham's F12 Medium containing 5% FBS, 2 mM glutamine, 50 ng/ml Penicillin/Streptomycin (all from Lonza, Switzerland), Choleratoxin (Sigma-Aldrich, MO), 10 μg/ml Insulin (Roche, Switzerland), 100 μg/ml Hydrocortisone (Sigma-Aldrich), and 20 ng/ml EGF (PeproTech, NJ) at 37°C in 5% CO_2. Cells were grown on glass coverslips, coated with gelatin 0.5% (wt/vol) in PBS, and, at 70% confluence, fixed for 10 min in 4% paraformaldehyde (wt/vol). To detect actively DNA-replicating cells, Ethinyl-deoxyuridine (EdU) (Life Technologies, CA) was added to the culture media (final concentration 10 μM) 40 min before fixation. After labeling, cells were washed twice with PBS and fixed as previously described.

Edu Staining and Immunofluorescence of MCF10A cells

For the 7-parameter widefield microscopy analysis, cells (including the cell lines shown in the Supporting Information Data Section) were permeabilized and processed using the Click-iT™ EdU Imaging kit (Life-Technologies) plus Pacific-Blue azide according to the manufacturer instructions.

After blocking (5% BSA in PBS), cells were incubated for 1 h at room temperature (RT) with primary antibodies [rabbit anti-53BP1 (ab36823 Abcam, UK) and mouse anti-p21 (M7202, Dako, Denmark)]. After washing (3×), they were incubated for 1 h at RT with anti-rabbit Pacific-Orange-conjugated IgGs (Life-Technologies) and anti-mouse Cy3-conjugated IgGs (Jackson Immuno-Research, UK). Cells were then refixed in 4% paraformaldehyde, blocked with 5% BSA containing mouse-IgG (Jackson Immuno-Research) and incubated for 1 h with the following mAbs: anti-KI67 Alexa647-conjugated (558615, BD Pharmingen, CA), anti-γH2AX Alexa488-conjugated (613406, Biolegend, CA), and anti-human p53 biotin-conjugated (DO1, Sigma-Aldrich). Finally, after washings, coverslips were incubated 1 h with CW800-conjugated anti-Biotin (600-132-098, Rockland, PA). DNA was counterstained with DAPI. Slides were then mounted in Mowiol-containing mounting media.

For the analysis of p63 expression, a putative stem-cell marker, the above-described protocol was modified using an anti-p63 mAb (sc-8431, Santa-Cruz, Germany) and anti-p21 biotin-conjugated antibody (ab79467, Abcam).

In Situ PLA

After EdU reaction (see below for details), samples were processed for in situ PLA according to manufacturer's instructions

(OLink Bioscience, Sweden) using the DuoLink in situ Orange detection reagent. Then, for complete detection of the expression levels of the targeted molecules, coverslips were incubated with fluorochrome conjugated antibodies (see previous section). Primary antibodies employed for PLA were: rabbit anti-53BP1 (ab36823, Abcam)/mouse anti-pH2AX (613402, Biolegend), rabbit anti-53BP1 (ab36823 Abcam)/mouse anti-p53 (sc-126, Santa Cruz), and goat anti-p53 (sc-6243, Santa Cruz)/mouse anti-pH2AX (613402, Biolegend). Secondary antibodies: Alexa488 anti-mouse and Alexa647 anti-rabbit or anti-goat conjugated antibodies.

For the detection of proximity between pH2AX and newly replicated DNA, EdU was detected by biotin-azide in place of the Pacific-Blue azide usually employed in the rest of the work. PLA primary coupled antibodies: rabbit anti-pH2AX (2212-1, Epitomics)/mouse anti-biotin (200-002-211, Jackson ImmunoResearch). DNA was counterstained with Chromomycin A3 (10 μM in PBS/70 mM MgCl2). Slides were mounted in DABCO-containing glycerol-based mounting media to preserve cell three-dimensional structures.

To verify the compatibility between the DNA-conjugated secondary antibodies employed for PLA and the secondary fluorochrome-conjugated antibodies, we measured the number of PLA foci before and after addition of fluorochrome-conjugated antibodies. No statistically significant differences were detected.

Automated Microscopy and Image Acquisition

Images were collected by a BX61 fully motorized Olympus fluorescence microscope controlled by Scan^R software (version 2.2.09, Olympus Germany). An oil-immersion 60× 1.3 NA objective was employed for acquisition.

The adopted fluorescence filter configuration is reported in the Supporting Information Table 1. Supporting Information Figure 1 reports the fluorescence distribution in the acquired channels for single-stained samples to demonstrate the absence of significant crosstalk.

Confocal microscopy data were collected with oil-immersion 40× 1.25 NA and 63× 1.4 NA objectives by a SP5 laser scanning spectral confocal microscope, equipped with a resonance scanning unit, and controlled by the Matrix routine for high content microscopy contained in the LAS software package (Leica Microsystems). More details on our acquisition procedure for cell relocalization can be found in this issue accompanying article.

Cell-Cycle Statistical Analysis

Cell identification was based on segmentation of DAPI nuclei signals and, thus, the analysis of all acquired parameters limited to nuclear expression and localization. First, false-cell events (over-fragmentation due to watershed based separation, cell aggregation, etc.) were excluded through analysis of physical (cell area and circularity) and fluorescence (mean and integrated density) parameters. Mitotic cells, identified by mean Dapi intensity versus cell area (high mean fluorescence due to DNA condensation and minimal dimension), or by mean fluorescence of DAPI versus KI67 (simultaneous high intensity due to DNA condensation and KI67 over-expression localized to chromosomes. See accompanying article by Furia et al.) were grouped into the corresponding DNA content (4N or 2N) populations, when not otherwise defined. Cell cycle phases were identified according to their DNA versus EdU integrated fluorescence intensity and EdU negative cells grouped according to their ploidy: 2N (G0/G1), midN (aneuploid cells), and 4N (G2M and G1 tetraploid) subpopulations. EdU positive cells were separated according to their EdU mean intensity level and DNA content in early S (2N and low-intermediate EdU content), S (high EdU intensity, independently of DNA content), and late S (4N and low-intermediate EdU content). The values obtained were used to perform cell-cycle related protein profiling, subdividing low and high expressing cells according to their spatial molecular density (mean fluorescence intensity per pixel). Evaluation of the mean fluorescence intensity (rather than the integrated) allowed exclusion of any nonspecific increase due to cell-volume growth during cell-cycle progression. Unlike flow-cytometry, which analyses global cell fluorescence, this image-related approach limits the noise generated by antibodies nonspecific binding and/or autofluorescence (strongly dependent on the cell area).

With the exception of a clear KI67 negative population, isolated and validated for complete absence of signal, negative controls (prepared with antibody isotypes, when available, or with serum, and incubated with the chosen secondary antibodies) systematically showed lower fluorescence values. Out-of-target primary antibody interactions at saturation and/or very small amounts of the target molecule challenged classical approaches for negative threshold settings. Since our goal was to get an indication on how to separate low and high range of expression, rather than absolute levels, we set an indicative threshold level by fitting the lower tail of the distribution in each channel by a Gaussian curve (Supporting Information Fig. 2), obtaining an R squared parameter (correlation between fitting and measured data) >0.9 in all the analyzed samples. A threshold was then set for each parameter at the 1% upper edge of the calculated distribution.

Low and high expressing cells were then classified according to the DNA-content reference-intervals previously established for the DNA versus EdU bivariate distribution (2N, mind, and 4N). All fluorescence values were normalized to the average value of the 2N low-expressing populations, for example, all the p21 values reported in the graphs were normalized to the mean p21 fluorescence of the 2N p21-low-expressing cell population.

Moreover, we employed image-analysis to monitor KI67 nucleolar localization as an additional marker of proliferation at low level of expression. In the KI67-negative cell population, KI67 total fluorescence intensity was comparable to the blank sample, but no nucleolar signal was present. Poorly expressing cells (KI67 low) showed fluorescence comparable or close to the blank threshold but with a detectable nucleolar accumulation, possibly indicating a commitment to proliferation.

For the γH2AX and 53BP1 DDR markers the integral of the intensities of all the detected foci per nucleus (Supporting Information Fig. 3) were considered in spite of γH2AX−, or in addition to 53BP1−, mean or integrated intensity per cell.

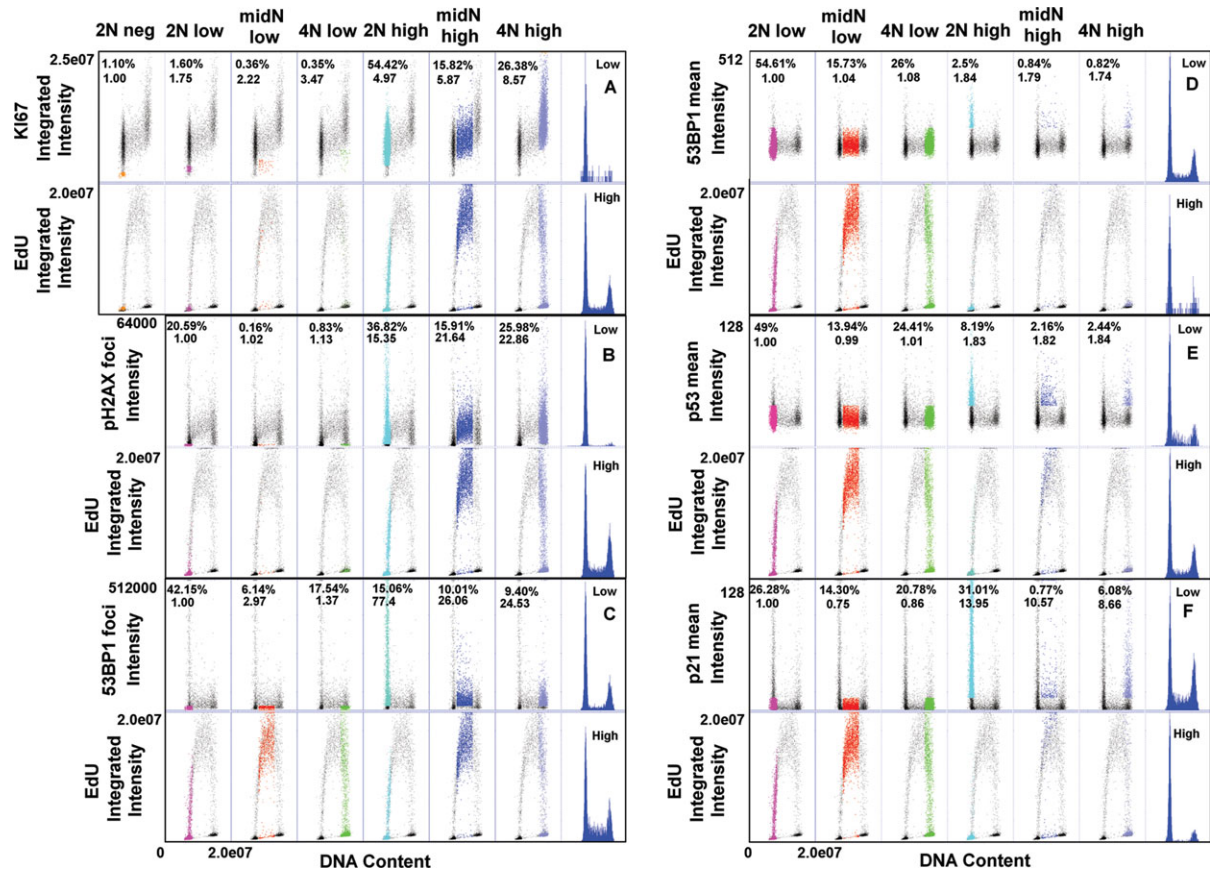

Figure 1. Seven parameter correlated analysis of DNA content, DNA replication, DNA damage response, and checkpoint activation provides population profiling to uncover cell-cycle specific modulation mechanisms. Exponentially growing MCF10A non-transformed human mammary cells were pulsed with EdU for 40 minutes prior fixation and stained for multiparametric image-cytometry analysis. DNA content (X axis) was correlated to the analysed parameters (Y axis): KI67 total intensity (A), gammaH2AX foci total intensity (B), 53BP1 foci total intensity(C), 53BP1 mean intensity per pixel (D), p53 mean intensity per pixel (E) and p21 mean intensity per pixel (F). Cell subpopulations (each one coded with a representative color) were definied according to the different ploidy and level of expression of the molecular marker as described in the Materials and Methods section, reporting percentage with respect to the total population and average level normalized to the 2N low expressing population in every channel. To analyze cell-cycle distribution for each parameter: i) the previously defined populations were relocated in the biparametric DNA vs EdU content multicolor plots (second row for each panel) and ii) DNA-profiles were plotted for low and high level expressing fractions. [Color figure can be viewed in the online issue, which is available at wileyonlinelibrary.com.]

The ratio between foci integrated fluorescence and the total intensity per nucleus was calculated and expressed as percentage. Foci were detected by applying a Laplace of Gaussian Filter to images to create a segmenting mask.

The software is also able to consider foci as statistically independent events without referring them to the cell of origin. Physical properties (area and circularity) and fluorescence related measurements identical to the ones acquired for cells (mean and integrated intensity) were also determined. Graphs report average values, and standard deviations were calculated from three independent experiments.

Results

Automated Microscopy Allows High-Content Protein Profiling of DDR, Checkpoint Activation, Proliferation Control, and Cell-Cycle Progression

We employed the high sensitivity and spectral-separation ability of the fluorescence microscope to set-up a seven-parameter analysis of some of the major molecular components involved in DDR and cell-cycle regulation.

Stoichiometric binding of a DNA dye (DAPI, widefield, or Chromomycin, confocal), allowed the classification of cells according to their ploidy, providing an indirect measurement of cell-cycle progression. Then, to separate actively replicating populations, cells were incubated with the Uridine-analogue EdU (41), its detection procedure being compatible with simultaneous immunostaining of intracellular antigens. Finally, proliferating and quiescent cells were separated according to the expression of the KI67 antigen (Fig. 1A). Thus, we were able to discriminate between cells in G0 (KI67 negative cells with 2N DNA content), G1 (2N DNA content, KI67 positive, EdU negative), S phase (EdU positive), and G2 (4N DNA content, EdU negative). DD evaluation was performed by simultaneous assessment of presence and intensity of γH2AX foci (Fig. 1B) and spatial localization and expression of the 53BP1 protein. For 53BP1, we considered separately the fluorescence

originated from the foci (Fig. 1C) and the nuclear signal (Fig. 1D) to distinguish between DDR-associated relocalization and total protein expression. Checkpoint activation was estimated by measuring p53 (Fig. 1E) and p21 (Fig. 1F) protein content.

Measurement of Physiological DNA-Damage in Relation to Cell Proliferation Unmasks DDR Independent Regulation of Cell-Cycle Entry/Exit

Absence of proliferation, measured from DNA/ KI67 distribution (Figs. 1A and 2A), was observed at different DNA contents ranging from 2N (G0/G1) up to 4N (G2M, tetraploid cells G0/G1 cells) at very low percentages (Fig. 2A). In the diploid quiescent population, negative G0 (Fig. 2A, KI67neg, Magenta) and poorly expressing G1 cells (Fig. 2A low, Red) were separated according to the complete absence/low presence of the expected KI67 nucleolar accumulation as described in the Methods section. Quiescence frequency outside the diploid compartment progressively decreased indicating that exit from the cell-cycle was mainly the result of a post-mitotic program (Fig. 2A). Indeed, quiescent fractions at midN and 4N DNA content might represent the G0/G1 phase of aneuploid populations as suggested by (i) EdU negativity and cyclin E (a G1 marker) expression in part of the population (data not shown) and (ii) the up-regulation of both p21 (Fig. 2D) and p53 (Fig. 2E). Unfortunately, due to the low number of events statistical analysis was not reliable.

Surprisingly, analysis of DDR and checkpoint markers in quiescent cells did not show a clear correlation. γH2AX (Fig. 2B) and 53BP1 (Fig. 2C) foci distribution revealed that levels of DDR activation were low in most quiescent cells (γH2AX and 53BP1foci intensities were low in 65 and 74% of cells, respectively). Even if we cannot exclude that the quiescent fraction was committed to future death, we did not observe any increase in γH2AX intensity to indicate the activation of an apoptic process, at least in the diploid compartment of the quiescent fraction. However, increased p21-expression was detected in all quiescent fractions (Fig. 2D), compared with their proliferating counterparts, independent of their DNA content and DDR response. However, by image-driven analysis, we noticed that p21 content quickly decreased when KI67 accumulation began in the nucleolus of KI67-low-expressing cells, suggesting the existence of intermediate stages between exit from the cell-cycle and full commitment to proliferation (Fig. 2D graph).

Remarkably, p53 activation (in association with high levels of DDR activation; Fig. 2E) was present in only 25% of quiescent cells, against p21 over-expression in 97.5% of them. Independently of its localization in foci, we also detected significant 53BP1 up-regulation in the quiescent population (Fig. 2F). Similarly, to p21, its mean content was dramatically higher in KI67-negative cells, progressively reducing after the cells began to express the proliferation antigen (Fig. 2F graph, KI67neg and low).

As previously published, mammary cell lines might contain rare subpopulations with phenotypic (marker expression) and functional (label retention) properties of stem cells (17). Since DDR-independent quiescence is a specific stem cell program, we analyzed the expression of the putative mammary stem-cell marker p63 (18) in our MCF10A quiescent (KI67-negative) subpopulation. Strikingly (Supporting Information Fig. 4), together with p21 and 53BP1, p63 levels were also significantly increased compared with proliferating cells, consistent with the existence of a quiescent program to preserve the self-renewing cell compartment.

Checkpoint Activation: Expression of Checkpoint Molecular Mediators in Relation to Cell-Cycle and DDR

Our analysis of quiescent cells suggests differences in the activation steps of the p53-p21 molecular pathways in the regulation of proliferative potential. Further analysis of the expression of these proteins in relation to cell-cycle profile (Figs. 1 and 3) showed that around 40% of all cells expressed high p21 levels, almost exclusively during the G1 (32%) and G2M (7%) phases (Figs. 1 and 3E). Analysis of p21 versus DNA content and mean EdU content confirmed its almost complete absence in actively replicating cells (about 5% of the entire p21 positive population): EdU incorporation immediately coincided with a significant decrease in p21 average content per cell (Fig. 3E).

On the contrary, beside the expected peaks in the G1 and G2 phases of the cell-cycle, p53 expression was partially maintained during DNA replication (Fig. 3D). A fraction of p53-positive cells, in fact, comparable to the one detected in G2, was maintained through the early and first half of the S-phase (4% of the entire population, equivalent to about 8% of the EdU positive fraction and 16% of the p53 high-expressing cells). We also examined 53BP1, which maintained a steady (average) level during all cell-cycle phases, with few 53BP1-up-regulated cells in G1 and G2 (Fig. 3G).

To dissect the underlying network hierarchy, we cross-analyzed phase by phase cell-populations with high levels of p53, p21, 53BP1, as well as γH2AX and 53BP1 foci (Supporting Information Fig. 5). The relative average protein content and the fraction of cells simultaneously expressing high-levels of proteins in the different populations were adopted as indicators. As explained in the "Material and Methods section," we arbitrarily set a threshold to distinguish different level of expression.

Notably, irrespective of the cell-cycle phase, p53 high-expression was always associated with DDR, but not always with p21 induction. Indeed, during the S phase, some of the cells maintained high p53-levels without concomitant increase in p21-content, suggesting the existence of mechanisms to monitor replication-associated damage recognition and/or processing. On the other hand, we detected a G1-specific p21-activation that was partially DDR and p53 independent. A more direct correlation between DDR and p21 was however observed as the cell-cycle proceeded.

Only a fraction of H2AX highly expressing cells were found to over-express either p53 or p21, suggesting the existence of an internal threshold for checkpoint activation. Finally, a p53-53BP1 circuit seemed to be maintained throughout the cell-cycle with the 53BP1 fraction consistently upregulating p53 (and p21).

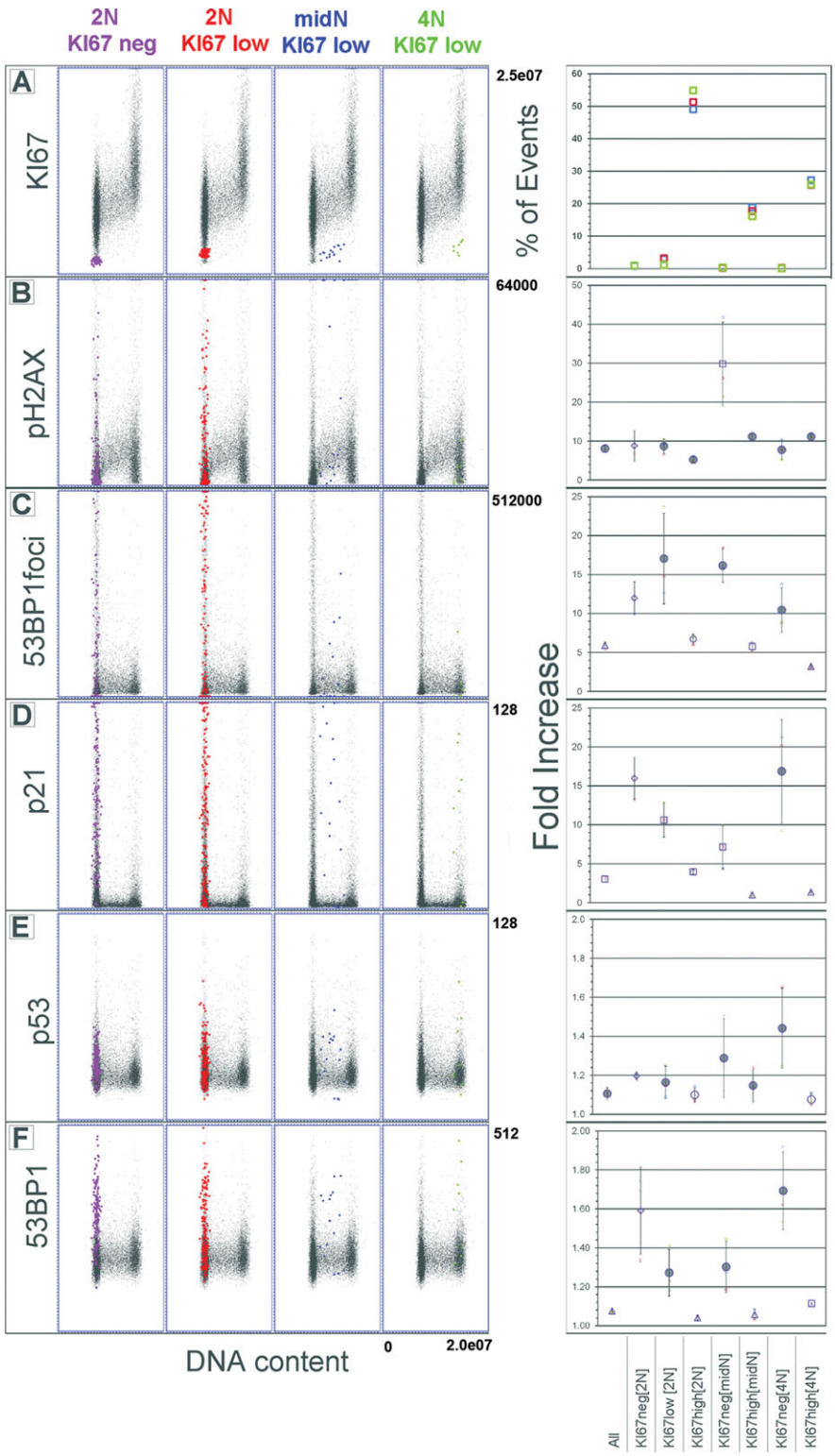

Figure 2. Identification and profiling of the proliferation marker KI67 shows the existence of a DDR-independent p21 and 53BP1 mediated quiescence program in a non-transformed cell line. Bivariate analysis of DNA and KI67 content per cell (A) was performed to identify different degrees of proliferating activity and their relation to cell-cycle. Image-guided determination of different KI67 expression levels was used to identify the resting fraction present in the analyzed exponentially growing population of cells. 2N KI67 negative cells (Magenta) presented undetectable localization of the antigen according to a fluorescence level comparable to blank reference sample. 2N KI67 low expressing cells (Red) showed instead a very weak, but discernible, staining in the nucleolar region. Quiescent populations were also identified at intermediate (Blue) and tetraploid (Green) DNA content. Multicolor Dot Plots evidenced the gammaH2AX (B) and 53BP1 (C) foci total intensity per cell, p53 (D), p21 (E), and 53BP1 (F) mean intensity per pixel. The graphs report percentages and fluorescence fold increase (average fluorescence intensity of the target population divided by the average intensity of the corresponding low-expressing subpopulation, see Materials and Methods) for every identified sub-population over three different experiments. [Color figure can be viewed in the online issue, which is available at wileyonlinelibrary.com.]

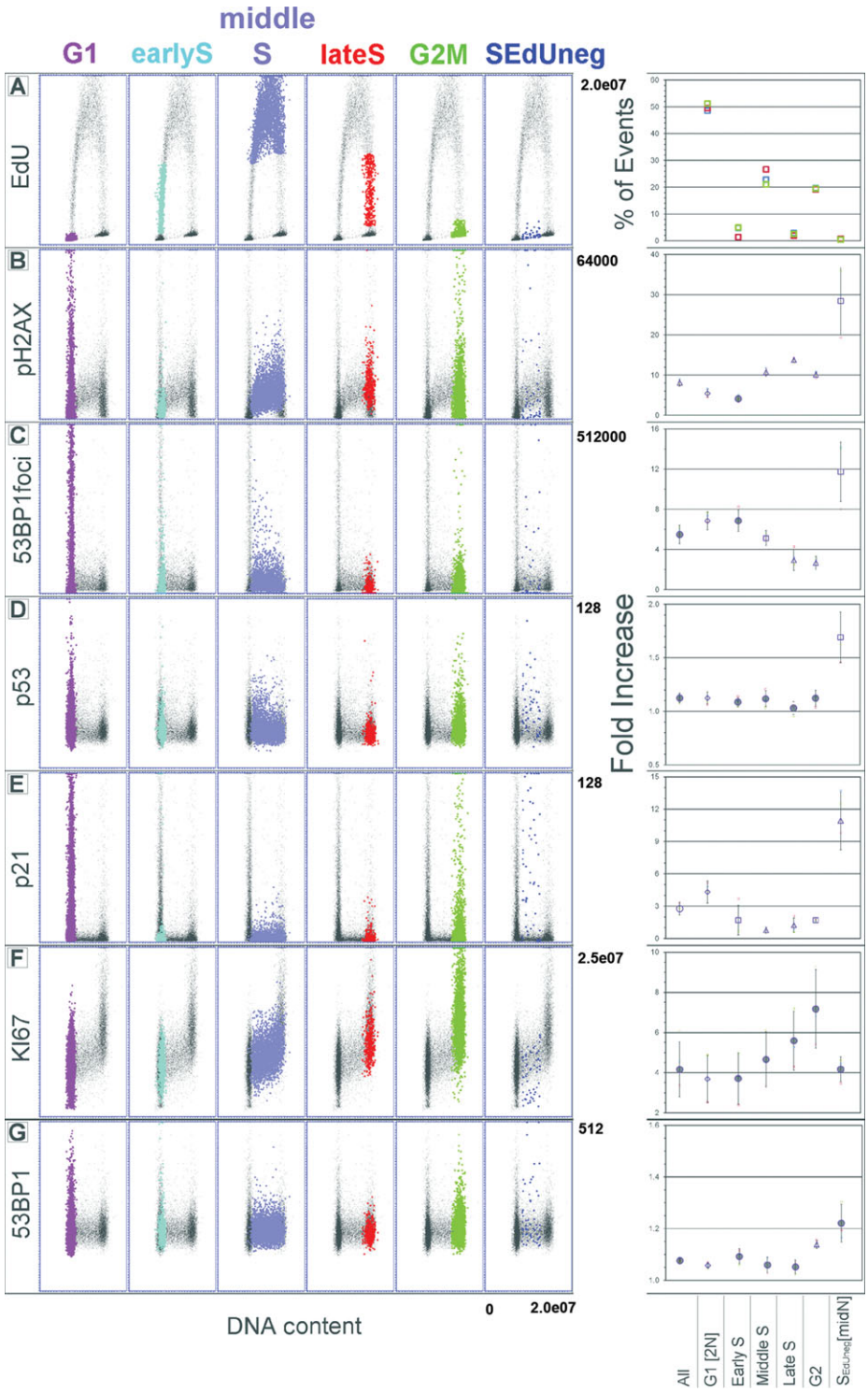

Figure 3. Correlated analysis of DNA content, replication activity, DDR and checkpoint marker expression during unperturbed cell growth. Bivariate analysis of DNA and EdU content per cell was performed to identify G1 (Magenta), actively replicating cells (early S, Cyan; Middle S, Violet; late S, Red) and G2M (Green). A replication inactive fraction with intermediate DNA content (SEdUneg, Blue) was clearly identified despite its low frequency. To characterize the specific phenotypes for each identified population, the relative distribution of the expression levels of the molecular targets of interest were calculated and visualized in the corresponding dot plot. The graphs report percentages and fluorescence fold increase (average fluorescence intensity of the target population divided by the average intensity of the corresponding low-expressing subpopulation, see Methods) for every identified subpopulation over three different experiments. [Color figure can be viewed in the online issue, which is available at wileyonlinelibrary.com.]

Cell-Cycle Distribution of the γH2AX and 53BP1 DD Markers Reflects Their Different Functional Roles in Damage Recognition and Repair

Correlation of replication activity and DDR showed opposite γH2AX- and 53BP1-foci kinetics profiles. As replication proceeded γH2AX-foci intensity per cell remained constantly higher than the positivity threshold (Fig. 3B, a), reaching its maximum during the late stages of the S phase when heterochromatin is replicated (42). This correlates with the hypothesis that the more condensed genomic regions require opening for DD to be recognized and processed. In G1 and G2M cells the γH2AX signal covered a wider range of values.

In contrast, the expression profile of the total intensity of 53BP1-foci per cell (Fig. 3C) showed a marked peak during G1, and a progressive decrease during DNA replication. Damaged cells in G2M regained, together with high γH2AX, increased 53BP1 recruitment into foci supporting its putative role in checkpoint activation (43,44).

To completely unmask differences in the morphology and composition, we measured the mean intensity and average size of 53BP1- and γH2AX-foci, confirming the existence of phenotypically distinct populations according to the cell-cycle stage. We then adopted two different approaches for the analysis of foci properties. First, we considered them as cell features and reported the average "ensemble" properties of all the foci pertaining to a single nucleus (Fig. 4: first and third columns). Secondly, we looked at the statistical distribution of the foci, considered as independent statistical events with their own physical and fluorescence properties (the cells of origin were only taken into account for their position in the cell cycle. Fig. 4: second and fourth columns). When examined either through the γH2AX or the 53BP1 channel, enlarged spots were observed in G1 cells, with sizes exceeding those reached in the other phases of the cycle (Fig. 4 G1), but disappearing as soon as cell replication began (compare G1 and early S panels). The behavior of the two markers, however, did not overlap: while γH2AX-foci maintained the same mean intensity, indicating a constant molecular density, enlarged 53BP1-foci clearly formed a separate population with a marked increase in the mean-pixel value suggesting a 53BP1-specific recruitment. To validate further, the hypothesis of different kinetics in foci formation, we analyzed γH2AX- and 53BP1-foci as independent statistical ensembles not hierarchically related to cells. Bivariate distributions showed the existence of a subset of γH2AX-foci not accumulating 53BP1. On the contrary, the entire 53BP1-foci population showed a good linear correlation between the intensities of the two markers (Supporting Information Fig. 6).

To validate the general nature of the observed cell-cycle related features of the observed phenotypes, we extended the analysis to a panel of cell lines (Supporting Information Table 2). Unfortunately, the analysis of p53 distribution is limited by its genetic and functional heterogeneity. The observed DDR-related features (γH2AX and 53BP1 foci cell-cycle distribution) were constantly reproduced in a normal (MRC5), non-transformed (MCF10A, BJ-Tert, HaCaT) and malignant background (HCT116, U2OS; Supporting Information Figs. 7 and 8). The p21 cell- cycle distribution and the DDR-independent increased expression of p21 during G1 was also maintained (Supporting Information Figs. 9 and 10). Similarly, a consistent fraction of the KI67-negative quiescent population (when present) did not show increased DDR markers (Supporting Information Fig. 11). However, in this case, no assumptions can be made on the presence of a self-renewing compartment.

High-Resolution Analysis of the Molecular Interactions Between DDR, Checkpoint-Activation, and DNA-Replication Networks

The observed relationships at cellular and intracellular level statistically inferred from the population analysis suggested a potential interaction between the analyzed molecular markers. To define the functional relationship linking DNA replication, damage induction, and damage recognition we employed in situ PLA (45), which allows cross-evaluation of the molecular proximity of replication factories, damage foci, and p53 spots. To optimize data collection, we designed a computer-aided acquisition protocol driving a confocal platform. Foci discrimination requires both optical-sectioning ability and adequate spatial oversampling satisfying the Nyquist rate in all the three dimensions, requirements not compatible with the large field of view imposed by the acquisition of thousands of cells. Consequently, in a first round of acquisition, low-resolution images of targeted channels were used to identify and isolate DNA replicating and/or p53 expressing cells (Fig. 5A). The corresponding stage coordinates were then employed to acquire selectively XYZ optimized single-cell image stacks to evaluate number and localization of interacting foci (Fig. 5B).

PLA analysis of the interaction between γH2AX and the incorporated EdU provided a measurement of the specificity of the assay: since EdU is not incorporated in G1 and G2M phases, the detected PLA signals could be attributed to aspecific interactions between the antibodies. The average number of non-specific foci was in the order of units or less, 10 times less than those detected during the S-phase (Fig. 5C: EdU vs. DNA and number of PLA foci vs. DNA). The proximity between EdU factories and γH2AX foci suggested a tight temporal correlation between DNA replication and H2AX phosphorylation. Correlation between γH2AX and 53BP1 showed that, despite their cell-cycle related differences in expression and spatial distribution, their molecular interaction could be detected at every stage of the cell-cycle. Regardless of its involvement in NHEJ repair activity, which is inhibited in S-phase, 53BP1 is not excluded from DDR during DNA replication. However, PLA analysis confirmed the existence of a fraction of visible foci in the γH2AX channel not involved in 53BP1 recruitment. It also revealed that p53 accumulation during the S-phase was concomitantly linked to damage processing, as the protein was associated to both the DNA-damage markers γH2AX and 53BP1. Strikingly, 53BP1-p53 interaction was clearly detected at different cell-cycle stages in a content-dependent manner, thus validating the correlation observed in the expression profiles.

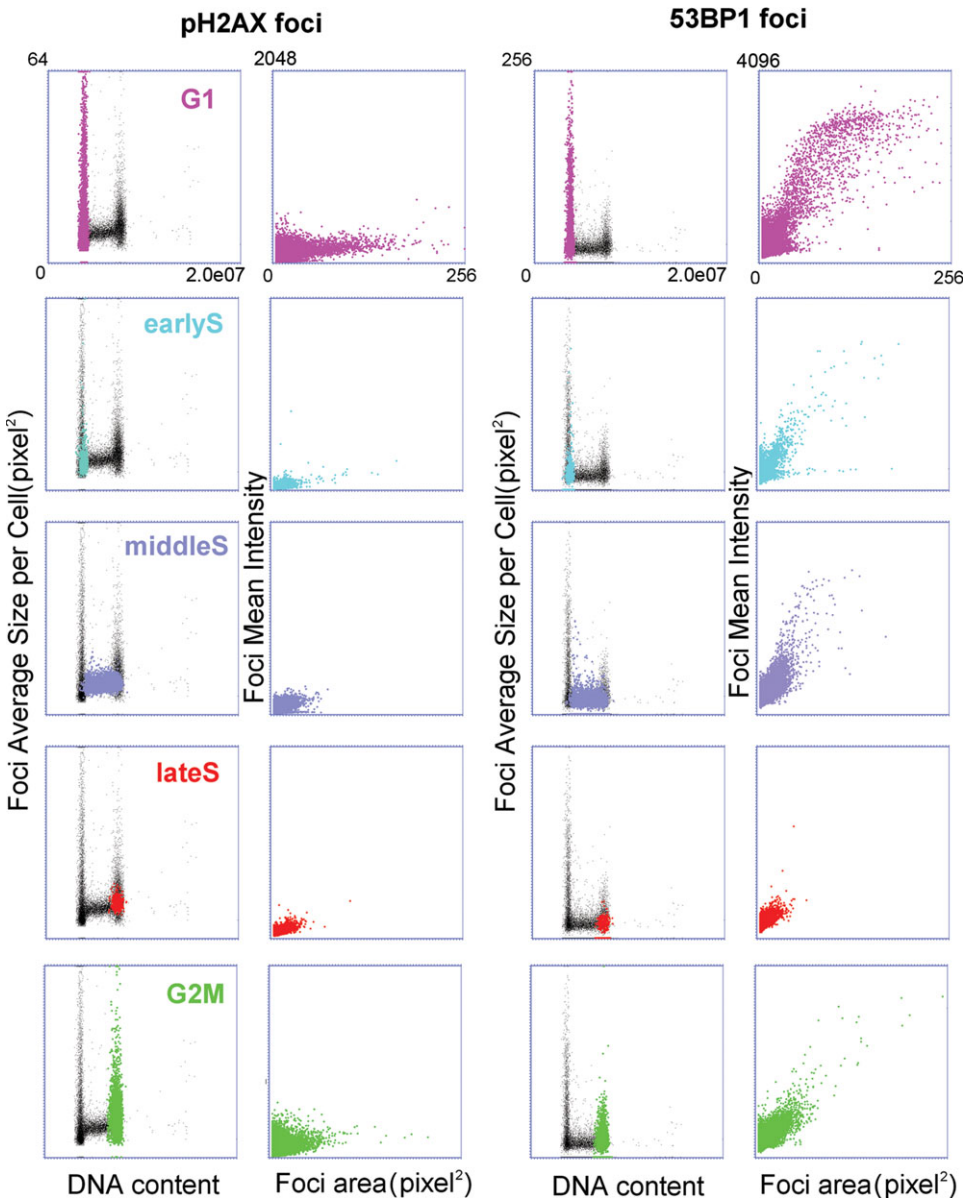

Figure 4. gammaH2AX and 53BP1 foci physical size varies according to the cell-cycle phase. Size of gammaH2AX (left panel) or 53BP1 (right panel) foci was analyzed at different stages of the cell-cycle. First column reports the average size of foci per cell while the second one shows the analysis of the entire foci population (note the difference in the Y-axis scale). Each row reports the distribution in the corresponding cell-cycle stage obtained by gating events according to the definition based on the DNA vs EdU content bivariate graph. [Color figure can be viewed in the online issue, which is available at wileyonlinelibrary.com.]

Discussion

Oncogene expression induces a hyperproliferation burst that causes an enhanced DNA-replication stress. The resulting DD can induce gene mutations and/or chromosomal aberrations, which may eventually lead to malignant transformation (46,47). To contrast this event the cells have developed physiological barriers by inducing a replicative senescence process, which is triggered by checkpoint activation via DDR. The goal of this study was to carry out a multiparameter analysis of replication-induced damage, cell-cycle regulation, proliferation, and DDR. Until now, this kind of high-content analysis was hindered by the lack of a comprehensive experimental approach, which could, at the same time, maintain single-cell resolution, high spatial-resolution, high-content, and statistical significance with respect to poorly represented phenotypes. In addition, cell-sorting manipulation and/or enhancement of specific cell features, usually employed to study DDR, carry the risk of potentially altering the physiological level of DNA-damage (29).

Herein, for the first time, we employed an image-cytometry computational platform to produce a multi-correlated quantitative cell-cycle profiling of both content and spatial

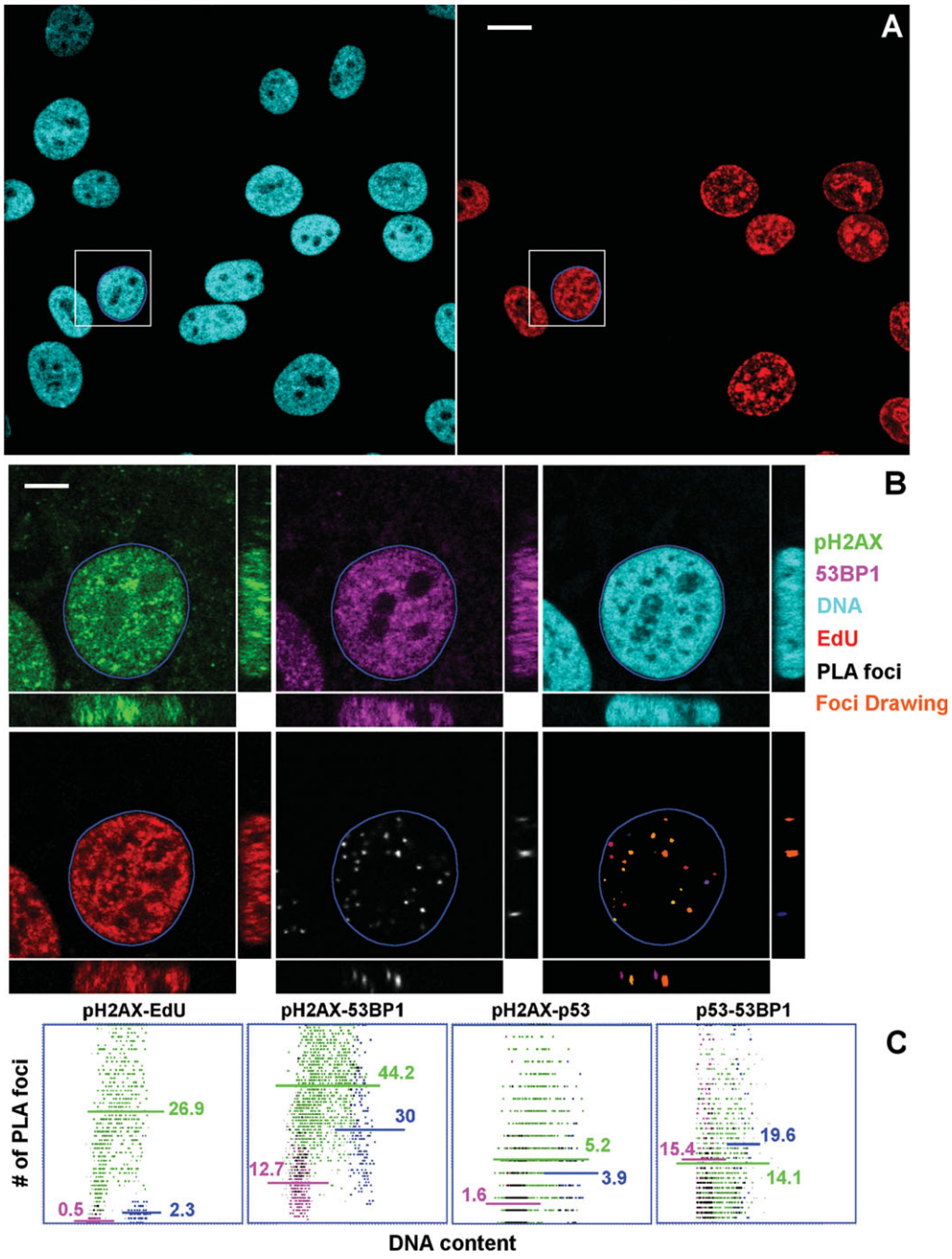

Figure 5. Combination of Proximity Ligation and image-analysis driven acquisition allows visualization of molecular interaction in intact cells subpopulations. Undersampled images (A) were collected with a confocal microscope to identify cell-cycle subpopulations of interest with a parallel analysis (Scale Bar: 12 μm). Stage coordinates were recalculated to proceed to a 3D oversampled acquisition extended to all the parameters of interest (Scale Bar: 5 μm). (B). Stacks were then used to calculate the distribution and average number (reported in the graph) of PLA foci in G1 (Magenta), G2(Blue) and S (Green) subpopulations. [Color figure can be viewed in the online issue, which is available at wileyonlinelibrary.com.]

distribution of DNA-replication (EdU), proliferation (KI67), DDR (γH2AX, 53BP1) and checkpoint activation (p53, p21) markers. Multiple cycles of data acquisition-analysis enabled us to assess the expression levels of these markers in the entire cell population, and their molecular interactions in single cells at the tens of nanometers range.

The analysis of γH2AX expression in relation to the cell-cycle phase and checkpoint activation showed, in an unperturbed context, an increased phosphorylation of this histone isoform during DNA replication. The analysis of different cell lines confirmed that this increase was not restricted to the MCF10A mammary cells but also present in other tissues and

in a malignant background. The pioneering work by P. Olive's group on the flow-cytometry analysis of γH2AX (26,34) had suggested cell-cycle modulation of H2AX phosphorylation. Our multiparameter approach has provided, through direct EdU labeling of S-phase cells, the detailed kinetics underlying this process: G1-early S and late S-G2 transition showed respectively the lowest and highest average γH2AX content within the cell-cycle. By scaling down from a cell-population to a molecular proximity level, we demonstrated that the observed γH2AX increase was partially responsible for activation of the DDR cascade, since only a fraction of foci exhibited simultaneous recruitment of the DDR-effector 53BP1. This provides further evidence of the limitations in the applicability of γH2AX as readout of the occurrence of DNA breaks (13–16).

However, if one considers the simultaneous presence of γH2AX and 53BP1 as an index of DDR activation following a DNA break, our results show a number of foci associated to replication that is very close to the number of endogenous DSBs expected for a single cell-cycle (about 50), and which has never been quantified before in-vivo at a single-cell resolution (48,49). PLA analysis also revealed the proximity of replication factories and γH2AX foci, thus suggesting that i) γH2AX S-phase signaling maybe associated to impaired progression of the replication-fork and that ii) the induced damage is immediately recognized by the DDR machinery. This interpretation is consistent with recent works, which, by laser-scanning cytometry and confocal microscopy, showed an S-phase specific γH2AX-induction at the replication sites in response to exogenous-oxidants treatment (32).

We demonstrated that the cell-cycle modulation of DDR, in the absence of exogenous DNA-damaging agents, cannot be inferred from the analysis of a single factor, e.g. γH2AX foci. DDR foci showed a higher level of heterogeneity in comparison to ionizing radiation induced foci, which show marked colocalization of 53BP1 and γH2AX. The comparison of γH2AX- and 53BP1-foci cell-cycle kinetics showed distinct profiles. In contrast with γH2AX-foci, no S-phase-induced increase in 53BP1-foci was detected, but we observed a strong accumulation of 53BP1-foci with specific properties (i.e., limited number, large average size, and high mean intensity) in G1. A detailed statistical analysis of the γH2AX- and 53BP1-foci as independent statistical entities showed the presence of distinct subpopulations as γH2AX accumulation was not necessarily accompanied by 53BP1 recruitment. This may be due to a temporally distinct recruitment of the two factors or to selective activation of a specific pathway restricted to γH2AX. Indeed, mitotic regulation of DDR signaling is reported limited to γH2AX accumulation with no 53BP1 binding to condensed chromosomes (50).

The activation of multiple repair modalities and the interplay with cell-cycle regulation mechanisms may justify the heterogeneity we observed by PLA in the content and protein interaction profile. 53BP1 protein is a key element in the NHEJ repair pathway, which is suppressed during DNA replication (51). However, the cell-cycle profile of γH2AX-53BP1 proximity showed a consistent number of PLA-foci suggesting the active participation of a fraction of 53BP1 molecules in DDR signaling during the S-phase. PLA of p53 provided a further confirmation of the complexity of the DDR network, which generates heterogeneous phenotypes in the γH2AX and 53BP1 response. Our data support p53 involvement in the replication-stress response in physiological conditions, up to now only measured under drug-induced replication-fork stalling (52). In fact, by PLA, we detected both p53 spatial proximity to γH2AX and 53BP1 foci and maintenance of high levels of p53 in a fraction of replicating cells. However, we observed a consistently higher number of p53-53BP1-foci than p53-γH2AX foci. This difference suggests that the interaction between p53 and 53BP1 may involve other pathway than the DDR (e.g., transcriptional modulation) and can extend to the whole cell-cycle. Moreover, measurement of the p21 content depicted a similar heterogeneous scenario evidencing both a p53-dependent role in the activation of the checkpoint and a damage independent function. Only a fraction of the cells with high p21 expression showed a simultaneous increase in γH2AX- and/or 53BP1-foci. p21 high-expressing cells not enriched in DDR foci could be the result of either p21 DNA repair activity or a p21, DDR-independent, function in cell cycle control. Strikingly, high levels of p21 were detected in a rare diploid cell-population not expressing the proliferation marker KI67, in the absence of detectable DDR activation. In this G0 subfraction, we also measured high levels of the p63 stem-cell marker, suggesting that p21 is required in these cells for the maintenance of quiescence and self-renewing capacity. Unexpectedly, as it has never been reported before, they also showed an increase in the average level of 53BP1. Since we did not detect any significant foci-accumulation, the higher concentration of 53BP1 in this quiescent population might be representative of a function of this protein in the maintenance of a stem-cell compartment and deserves further investigation.

In conclusion, the application of our high-content, high-resolution, automated Image Cytometry protocol allows the identification of rare cell subpopulations, such as stem cells, and can provide an invaluable quantitative tool for cell biology studies. Importantly, biological heterogeneity can be analyzed without the introduction of exogenous agents, thus avoiding any potential interference with the selected molecular targets. The intrinsic high-content potential of this technique might also be used to create an unprecedented data-reservoir for in silico system biology.

Acknowledgments

The authors thank Massimo Scauso and Paolo Sapuppo for their support in system set-up and helpful discussions. They are indebted to Stefano Campaner, Ivan Dellino, Daniel Krueger, and Dario Parazzoli for critical discussions. They also thank Francesca Ballarini and Paola Dalton for critical revision of the manuscript.

Literature Cited

1. Halazonetis TD, Gorgoulis VG, Bartek J. An oncogene-induced DNA damage model for cancer development. Science 2008;319:1352–1355.
2. Jackson SP, Bartek J. The DNA-damage response in human biology and disease. Nature 2009;461:1071–1078.

3. Lamarche BJ, Orazio NI, Weitzman MD. The MRN complex in double-strand break repair and telomere maintenance. FEBS Lett 2010;584:3682–3695.
4. Kim JE, Minter-Dykhouse K, Chen J. Signaling networks controlled by the MRN complex and MDC1 during early DNA damage responses. Mol Carcinog 2006;45:403–408.
5. Lisby M, Rothstein R. Choreography of recombination proteins during the DNA damage response. DNA Repair (Amst) 2009;8:1068–1076.
6. Rupnik A, Lowndes NF, Grenon M. MRN and the race to the break. Chromosoma 2010;119:115–35.
7. Darzynkiewicz Z, Traganos F, Zhao H, Halicka HD, Skommer J, Wlodkowic D. Analysis of individual molecular events of DNA damage response by flow- and image-assisted cytometry. Methods Cell Biol 2011;103:115–147.
8. Tanaka T, Halicka D, Traganos F, Darzynkiewicz Z. Cytometric analysis of DNA damage: Phosphorylation of histone H2AX as a marker of DNA double-strand breaks (DSBs). Methods Mol Biol 2009;523:161–168.
9. Beck H, Menzel T, Syljuasen RG, Sorensen CS. High-throughput siRNA screens using gammaH2AX as marker uncover key regulators of genome integrity in mammalian cells. Cell Cycle 2010;9:2257–2258.
10. Lowndes NF, Toh GW. DNA repair: The importance of phosphorylating histone H2AX. Curr Biol 2005;15:R99–R102.
11. Mah LJ, El-Osta A, Karagiannis TC. gammaH2AX: A sensitive molecular marker of DNA damage and repair. Leukemia 2010;24:679–686.
12. Srivastava N, Gochhait S, de Boer P, Bamezai RN. Role of H2AX in DNA damage response and human cancers. Mutat Res 2009;681:180–188.
13. Cleaver JE. gammaH2Ax: Biomarker of damage or functional participant in DNA repair "all that glitters is not gold!". Photochem Photobiol 2011;87:1230–1239.
14. Cleaver JE, Feeney L, Revet I. Phosphorylated H2Ax is not an unambiguous marker for DNA double-strand breaks. Cell Cycle 2011;10:3223–3224.
15. de Feraudy S, Revet I, Bezrookove V, Feeney L, Cleaver JE. A minority of foci or pan-nuclear apoptotic staining of gammaH2AX in the S phase after UV damage contain DNA double-strand breaks. Proc Natl Acad Sci USA 2010;107:6870–6875.
16. Revet I, Feeney L, Bruguera S, Wilson W, Dong TK, Oh DH, Dankort D, Cleaver JE. Functional relevance of the histone gammaH2Ax in the response to DNA damaging agents. Proc Natl Acad Sci USA 2011;108:8663–8667.
17. Takahashi A, Ohnishi T. Does gammaH2AX foci formation depend on the presence of DNA double strand breaks? Cancer Lett 2005;229:171–179.
18. Goodarzi AA, Jeggo P, Lobrich M. The influence of heterochromatin on DNA double strand break repair: Getting the strong, silent type to relax. DNA Repair (Amst) 2010;9:1273–1282.
19. Goodarzi AA, Noon AT, Jeggo PA. The impact of heterochromatin on DSB repair. Biochem Soc Trans 2009;37:569–576.
20. Langerak P, Russell P. Regulatory networks integrating cell cycle control with DNA damage checkpoints and double-strand break repair. Philos Trans R Soc Lond B Biol Sci 2011;366:3562–3571.
21. Bouwman P, Aly A, Escandell JM, Pieterse M, Bartkova J, van der Gulden H, Hiddingh S, Thanasoula M, Kulkarni A, Yang Q, et al. 53BP1 loss rescues BRCA1 deficiency and is associated with triple-negative and BRCA-mutated breast cancers. Nat Struct Mol Biol 2010;17:688–695.
22. Bunting SF, Callen E, Wong N, Chen HT, Polato F, Gunn A, Bothmer A, Feldhahn N, Fernandez-Capetillo O, Cao L, et al. 53BP1 inhibits homologous recombination in Brca1-deficient cells by blocking resection of DNA breaks. Cell 2010;141:243–254.
23. Harrigan JA, Belotserkovskaya R, Coates J, Dimitrova DS, Polo SE, Bradshaw CR, Fraser P, Jackson SP. Replication stress induces 53BP1-containing OPT domains in G1 cells. J Cell Biol 2011;193:97–108.
24. Lukas C, Savic V, Bekker-Jensen S, Doil C, Neumann B, Pedersen RS, Grofte M, Chan KL, Hickson ID, Bartek J, et al. 53BP1 nuclear bodies form around DNA lesions generated by mitotic transmission of chromosomes under replication stress. Nat Cell Biol 2011;13:243–253.
25. Fernandez-Capetillo O, Chen HT, Celeste A, Ward I, Romanienko PJ, Morales JC, Naka K, Xia Z, Camerini-Otero RD, Motoyama N, et al. DNA damage-induced G2-M checkpoint activation by histone H2AX and 53BP1. Nat Cell Biol 2002;4:993–997.
26. Yu T, MacPhail SH, Banath JP, Klokov D, Olive PL. Endogenous expression of phosphorylated histone H2AX in tumors in relation to DNA double-strand breaks and genomic instability. DNA Repair (Amst) 2006;5:935–946.
27. Gerashchenko BI, Dynlacht JR. A tool for enhancement and scoring of DNA repair foci. Cytometry Part A 2009;75A:245–252.
28. Darzynkiewicz Z, Halicka DH, Tanaka T. Cytometric assessment of DNA damage induced by DNA topoisomerase inhibitors. Methods Mol Biol 2009;582:145–153.
29. Darzynkiewicz Z, Halicka HD, Zhao H, Podhorecka M. Cell synchronization by inhibitors of DNA replication induces replication stress and DNA damage response: Analysis by flow cytometry. Methods Mol Biol 2011;761:85–96.
30. Huang X, Halicka HD, Traganos F, Tanaka T, Kurose A, Darzynkiewicz Z. Cytometric assessment of DNA damage in relation to cell cycle phase and apoptosis. Cell Prolif 2005;38:223–243.
31. Tanaka T, Huang X, Halicka HD, Zhao H, Traganos F, Albino AP, Dai W, Darzynkiewicz Z. Cytometry of ATM activation and histone H2AX phosphorylation to estimate extent of DNA damage induced by exogenous agents. Cytometry Part A 2007;71A:648–661.
32. Zhao H, Dobrucki J, Rybak P, Traganos F, Dorota Halicka H, Darzynkiewicz Z. Induction of DNA damage signaling by oxidative stress in relation to DNA replication as detected using "click chemistry". Cytometry Part A 2011;79A:897–902.
33. Zhao H, Traganos F, Darzynkiewicz Z. Kinetics of the UV-induced DNA damage response in relation to cell cycle phase. Correlation with DNA replication. Cytometry Part A 2010;77A:285–293.
34. MacPhail SH, Banath JP, Yu Y, Chu E, Olive PL. Cell cycle-dependent expression of phosphorylated histone H2AX: Reduced expression in unirradiated but not X-irradiated G1-phase cells. Radiat Res 2003;159:759–767.
35. Cai Z, Vallis KA, Reilly RM. Computational analysis of the number, area and density of gamma-H2AX foci in breast cancer cells exposed to (111)In-DTPA-hEGF or gamma-rays using Image-J software. Int J Radiat Biol 2009;85:262–271.
36. Gonzalez JE, Lee M, Barquinero JF, Valente M, Roch-Lefevre S, Garcia O. Quantitative image analysis of gamma-H2AX foci induced by ionizing radiation applying open source programs. Anal Quant Cytol Histol 2012;34:66–71.
37. Ishikawa A, Yamauchi M, Suzuki K, Yamashita S. Image-based quantitative determination of DNA damage signal reveals a threshold for G2 checkpoint activation in response to ionizing radiation. Genome Integr 2010;1:10.
38. Jucha A, Wegierek-Ciuk A, Koza Z, Lisowska H, Wojcik A, Wojewodzka M, Lankoff A. FociCounter: A freely available PC programme for quantitative and qualitative analysis of gamma-H2AX foci. Mutat Res 2010;696:16–20.
39. Mistrik M, Oplustilova L, Lukas J, Bartek J. Low-dose DNA damage and replication stress responses quantified by optimized automated single-cell image analysis. Cell Cycle 2009;8:2592–2599.
40. Hou YN, Lavaf A, Huang D, Peters S, Huq R, Friedrich V, Rosenstein BS, Kao J. Development of an automated gamma-H2AX immunocytochemistry assay. Radiat Res 2009;171:360–367.
41. Salic A, Mitchison TJ. A chemical method for fast and sensitive detection of DNA synthesis in vivo. Proc Natl Acad Sci USA 2008;105:2415–2420.
42. Chagin VO, Stear JH, Cardoso MC. Organization of DNA replication. Cold Spring Harb Perspect Biol 2010;2:a000737.
43. Shibata A, Barton O, Noon AT, Dahm K, Deckbar D, Goodarzi AA, Lobrich M, Jeggo PA. Role of ATM and the damage response mediator proteins 53BP1 and MDC1 in the maintenance of G(2)/M checkpoint arrest. Mol Cell Biol 2010;30:3371–3383.
44. Stiff T, Cerosaletti K, Concannon P, O'Driscoll M, Jeggo PA. Replication independent ATR signalling leads to G2/M arrest requiring Nbs1, 53BP1 and MDC1. Hum Mol Genet 2008;17:3247–3253.
45. Leuchowius KJ, Weibrecht I, Soderberg O. In situ proximity ligation assay for microscopy and flow cytometry. Curr Protoc Cytom 2011;Chapter 9:Unit 9 36.
46. Mallette FA, Ferbeyre G. The DNA damage signaling pathway connects oncogenic stress to cellular senescence. Cell Cycle 2007;6:1831–1836.
47. Mallette FA, Gaumont-Leclerc MF, Ferbeyre G. The DNA damage signaling pathway is a critical mediator of oncogene-induced senescence. Genes Dev 2007;21:43–48.
48. Vilenchik MM, Knudson AG. Endogenous DNA double-strand breaks: Production, fidelity of repair, and induction of cancer. Proc Natl Acad Sci USA 2003;100:12871–12876.
49. Zhao H, Tanaka T, Halicka HD, Traganos F, Zarebski M, Dobrucki J, Darzynkiewicz Z. Cytometric assessment of DNA damage by exogenous and endogenous oxidants reports aging-related processes. Cytometry Part A 2007;71A:905–914.
50. Giunta S, Belotserkovskaya R, Jackson SP. DNA damage signaling in response to double-strand breaks during mitosis. J Cell Biol 2010;190:197–207.
51. Lowndes NF. The interplay between BRCA1 and 53BP1 influences death, aging, senescence and cancer. DNA Repair (Amst);9:1112–1116.
52. Sengupta S, Linke SP, Pedeux R, Yang Q, Farnsworth J, Garfield SH, Valerie K, Shay JW, Ellis NA, Wasylyk B, et al. BLM helicase-dependent transport of p53 to sites of stalled DNA replication forks modulates homologous recombination. EMBO J 2003;22:1210–1222.